Resolution limits from charge transport in optically addressed spatial light modulators

Li Wang and Garret Moddel[a)]
Department of Electrical and Computer Engineering and Center for Optoelectronic Computing Systems,
University of Colorado, Boulder, Colorado 80309-0425

Spatial resolution of optically addressed spatial light modulators (OASLMs) is degraded by several different transfer processes in these devices. We have developed a general transient charge transport model to calculate and simulate the resolution limits of OASLMs due to the following charge spreading mechanisms during the transfer process in which the input image is converted into a particular charge distribution in the photosensor layer. (i) The effect of charge drift in the photosensor bulk on resolution increases with the thickness of the photosensor and the light-modulating layers. It also increases with the total amount of photogenerated charge collected at the interface. (ii) The effect of charge diffusion in the photosensor bulk on resolution is largely independent of the carrier mobility in the semiconductor photosensor. In most cases the corresponding spatial frequency $f_{50\%}$ is proportional to $\sqrt{V_{sc}}/d_{sc}$, where d_{sc} is the photosensor thickness and V_{sc} is the voltage drop in that layer. To have high-sensitivity OASLMs the transit time of charge carriers from the photosensor bulk to the interface must be much shorter than the recombination lifetime. (iii) The effects that charge drift, diffusion, and trapping at the photosensor-light-modulating layer interface have on resolution depend strongly on the interface properties. Decreasing the mobility or the trapping time of charge carriers at the interface can dramatically improve the resolution of OASLMs. The resolution ranges from 3 to 875 line pairs/mm for respective diffusion lengths of 10 to 0.1 μm at the interface. The combined effect on resolution from each of the charge spreading and other resolution-degrading mechanisms is also discussed. © *1995 American Institute of Physics.*

I. INTRODUCTION

Optically addressed spatial light modulators (OASLMs) are real-time optical signal transducers. The output from these devices is spatially and temporally modulated by the input image. There are several different OASLM structures including liquid crystal (LC)-semiconductor devices,[1-4] multiple quantum well (MQW) modulators,[5,6] and Pockels readout modulators (PROMs).[7,8] Their applications include high resolution displays, image processing, and optical computing.[9] In these devices electron-hole pairs are generated by the incident photons in the photosensitive layers. They are separated by the applied electric field and accumulate at the semiconductor-LC interface or semiconductor-dielectric mirror interface in the LC OASLMs, or two opposite semiconductor-dielectric interfaces in MQW modulators and PROMs. The electric field in the modulating layer is determined by the interface charge, or bulk charge distribution. The output light beam passing through the modulating layer is modulated accordingly. The modulating layer may be the LC or the photosensitive layer itself.

One of the crucial performance parameters in these devices is spatial resolution. It is determined by several transfer processes which include the transfer characteristic of input image modulation to interface or bulk charge distribution, to the voltage distribution, and finally to the output image modulation. Various models have been developed to predict and evaluate the theoretical resolution limits. Modulation transfer functions (MTFs) from input image to output image in PROMs have been successfully simulated by considering the fringing field effect, or drift of charge carriers in the bulk semiconductor layer.[10] Another charge-transport model has also been developed that takes into account charge drift and diffusion effects that occur during steady-state operation of MQW modulators.[11] If the charge spreading effects are negligible, then electro-static models[12,13] can be used to evaluate the resolution of OASLMs based on the transfer process from interface, or bulk charge distribution to voltage distribution, which give the thickness-dependence of MTFs. One such model has been developed to include devices with multi-layer structures.[14] Similar to the electro-static models, the voltage distribution at the semiconductor-LC interface can also be calculated by considering the conductivities of the LC layer and the dark and the illuminated regions of semiconductor layer in OASLMs.[15]

Since the charge carrier generation and accumulation from the input image involve various charge transport processes in the bulk region and at the interface, it is expected that charge spreading is inevitable in these processes and it will deteriorate the spatial resolution of OASLMs. In some LC OASLMs[16] the measured MTF curves fit the electro-static model[12] very well. This indicates that the resolutions of these devices are limited by the transfer process from charge distribution to voltage distribution. In other devices with similar structures,[2,17] the measured resolutions are much lower than the predictions from the electro-static models, and appear to be limited by charge spreading effects. Usually LC OASLMs and MQW modulators are operated under ac elec-

[a)]Electronic mail: moddel@boulder.colorado.edu

tric fields with 1–100 kHz frequencies. The charge distribution in the photosensitive layer varies with time, as does the voltage in the light-modulating layer. Therefore it is crucial to model the *transient* charge transport and understand its effect on resolutions of OASLMs. In this article a comprehensive charge transport model is developed for OASLMs that do not have patterned pixels. It includes charge diffusion and drift in the bulk region and at the interface. Effects of charge carrier recombination and trapping during the transport process are also discussed. The model does not predict the charge spreading effect that occurs when the OASLMs are operated near the saturation regime, in which highly nonlinear charge transport processes may occur. The model is restricted to the two-layer structure for the purpose of analytical tractability, but it can be generalized to a three-layer structure that is completely suitable for three-layer MQW modulators. It is difficult if not impossible to solve a series of three-dimensional rate equations regarding the charge transport process. Instead the charge transport is divided into several separate processes and the effect of each process on resolution is calculated and compared. The fringing field effect is discussed first. It deals with drift of the charge carriers in the bulk region during their transit. The effect on the spatial resolution of charge diffusion in the bulk is discussed by solving the two-dimensional rate equations. Finally, charge carrier transport at the interface between the semiconductor and the dielectric or LC layer is described with a simple, analytic model, and also with a complete numerical model. The MTF, which is suitable for the linear bulk diffusion effect, and an effective MTF, which is defined in this article for the nonlinear fringing field effect and the charge spreading at the interface, are used to characterize the effects of these processes on the resolution of OASLMs. The contrast transfer function (CTF) is also discussed (in Appendix A) for comparison and completeness.

In Sec. II the details of the charge spreading mechanisms are given, and methods to characterize them are introduced. The effect of fringing fields is discussed in Sec. III, followed by the evaluation of diffusion in the bulk in Sec. IV. Section V concentrates on charge spreading at the interface, followed by a discussion and conclusions in Sec. VI.

II. CHARGE SPREADING MECHANISMS AND THEIR CHARACTERIZATION

The development of the theory and modeling is based on a LC OASLM structure, but the results are applicable to MQW modulators and PROMs as long as some modifications are made. These will be discussed in relevant sections.

A schematic diagram of a typical LC OASLM is shown in Fig. 1. The device consists of a photosensitive semiconductor layer and a LC thin film. They are sandwiched between two transparent electrodes. In devices with crystalline semiconductor photosensors the semiconductor is usually undoped or slightly doped in order to be fully depleted during operation.[1,18] The devices are driven in alternating write (charge depletion) and reset (charge accumulation) periods of a square wave. At the beginning of the write period most of the applied voltage is dropped across the depletion region in the semiconductor layer. The amplitude of the voltage across
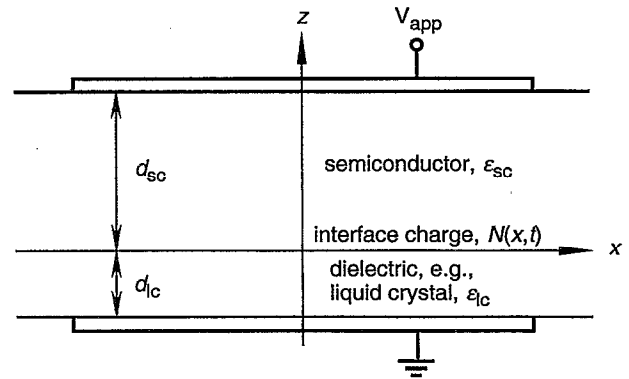

FIG. 1. Schematic cross section of an optically addressed spatial light modulator. The thicknesses and dielectric constants of the semiconductor and liquid crystal layers are d_{sc}, d_{lc}, ϵ_{sc}, and ϵ_{lc}, respectively.

the LC is small. When the write light is incident on the device electron-hole pairs are generated by incident photons in the depletion region and separated by the electric field. Some of the charge carriers are deposited at the semiconductor-LC interface, while the opposite-sign charge carriers drift toward the electrode. The voltage across the LC is spatially modulated as a consequence of the charge distribution. Therefore a readout light beam passing through the LC film will be modulated accordingly. In the reset period the interface charge is swept out by the applied reset electric field and recombines with opposite-sign carriers in the bulk region and at the electrode. Any charge image created in a previous write period is completely erased at the end of the reset period. In some hydrogenated amorphous silicon (*a*-Si:H) OASLMs the semiconductor layer has a *p-i-n* structure with the *n* layer at the LC interface.[2] These OASLMs are operated in the same way except that in the write period the initial voltage across the LC film can be adjusted by changing the applied voltage in previous reset period.[19,20] Charge carriers deposited at the LC-*a*-Si:H photosensor interface are electrons. Because the electrons, which have much higher mobilities than holes, are carriers which are transported through the photosensor, this configuration results in devices with shorter response times than the reverse configuration (*n-i-p*).

In the write period the photo-generated charge carriers drift under the electric field that is determined by the applied voltage and interface charge distribution. Therefore the carriers follow the electric field lines and are deposited at the interface.[3,10] Usually the electric field is not uniform and the field lines are not perpendicular to the electrode/interface anywhere due to the existing spatially varying charge distribution at the interface. Thus even though the spatial distribution of photo-generated charge carriers may be exactly proportional to the intensity pattern of the input image the resulting interface charge will deviate from the original input light intensity distribution due to this fringing field effect. The lateral electric field moves charge carriers from high concentration regions to low concentration regions. This reduces the modulation depth of the interface charge distribu-

L. Wang and G. Moddel

tion, and therefore the overall spatial resolution of the device decreases.

Other charge transport processes in the bulk region are diffusion and recombination, which occur during the transit. Diffusion is caused by the nonuniform distribution of photo-generated charge carriers in space. These carriers also recombine with opposite-sign charge carriers. These processes further reduce the modulation depth of the resulting interface charge distribution.

The surviving charge carriers arriving at the interface may diffuse and drift laterally due to the existence of charge nonuniformities and lateral electric fields until they become trapped by interface states or induced opposite-sign charge from the LC. This charge spreading process strongly depends upon the properties of the interface and will be discussed in detail in following sections.

In any of the above charge transport processes an input charge distribution which is symmetrical about the z axis or an even function of the coordinate x results in a final charge distribution that keeps the same parity due to the symmetry of the device structure about the z axis. In the following sections it is implicitly assumed that the input charge distribution for each transport process is a periodic, even function. Therefore the resulting charge distribution must be an even function having the same period. Such a function can be expanded in a Fourier cosine series.

One of the common ways to evaluate the resolution characteristics in an optical imaging system is the MTF measurement with sinusoidal input.[21] The MTF is the ratio of the modulation in the output image intensity to that in the input image intensity, and it usually decreases with spatial frequency. We can apply the same principle to the charge transport process and use the MTF to characterize the effects of charge spreading on OASLM resolution. The MTF, however, is well defined only for a linear transfer process, such as the bulk diffusion. Charge spreading due to drift, both in the bulk and at the interface, are generally nonlinear processes due to the presence of charge-induced fields. The MTF is no longer strictly valid for these processes, but we can still use the MTF concept to evaluate the charge spreading effects by defining an "effective MTF". For an input charge distribution or a charge generation rate having a sinusoidal-wave shape with modulation of m_{in}, we define the average and the first harmonic amplitudes in the output charge distribution as N_{out0} and N_{out1}, respectively. Then the effective modulation in the output charge is given by $m_{out} = N_{out1}/N_{out0}$. The effective MTF for this charge spreading process can be defined as $MTF_{eff} = m_{out}/m_{in}$. The definition of MTF_{eff} is consistent with the small amplitude modulation approximation in which the higher order harmonics in the output are neglected. The MTF_{eff} depends upon the average input charge density and its modulation m_{in}. The MTF_{eff} reduces to the MTF for a linear transfer process. Both the MTF and the MTF_{eff} will be used in the following sections.

The CTF could also be used to characterize the charge spreading effects. We have found in carrying out the numerical calculations of the following sections that the CTF and the MTF_{eff} give very similar results. Therefore we use only the MTF_{eff} and relegate the definition and numerical calculation results for the CTF to Appendix A.

III. FRINGING FIELD EFFECT

In order to isolate the fringing field effect from other charge transport processes and to investigate it alone, the following assumptions and facts have been made and restated:

(1) The bulk semiconductor region is electrically neutral. This assumption holds well only in crystalline semiconductors with low doping. In a-Si:H and some other semiconductors photo-generated holes are immobile or have very small mobilities. This creates space charge, which complicates the voltage distribution.

(2) Charge carriers are generated at the semiconductor-electrode interface. This assumption is valid if the input light beam is incident from this side and the absorption length is small compared with the semiconductor thickness.

(3) The path that charge carriers follow as they drift towards the interface is along the electric field lines that are built up by previously accumulated interface charge. This fact is justified by the linear relationship between drift velocity and electric field $v = \mu E$.

(4) Charge carriers generated at the same time will arrive at the semiconductor-LC interface simultaneously. This assumption is valid if the lateral (i.e., parallel to the surface) electric field in the bulk region is small compared with the vertical component. The transit time is relatively uniform across the entire active area. This does not necessarily mean that the effect of fringing field on resolution becomes small when the lateral electric field is reduced, as will become evident in following discussion.

(5) Once charge carriers arrive at the interface they stay there permanently, i.e., until the reset period. The charge distribution at the interface is calculated iteratively following the above assumptions and facts.

The periodic interface charge carrier concentration $N(x)$ with fundamental radial spatial frequency v may be expressed as

$$N(x) = N_0 + \sum_{n=1}^{\infty} N_n \cos(nvx), \qquad (1)$$

where N_0 and N_n are the average and nth Fourier-cosine component in the carrier distribution. Using Poisson's equation, the electric potential $V(x,z)$ in bulk region is found to be[12]

$$V(x,z) = \frac{V_0(\epsilon_{lc}z + \epsilon_{sc}d_{lc}) + qN_0(d_{sc}d_{lc} - zd_{lc})}{\epsilon_{lc}d_{sc} + \epsilon_{sc}d_{lc}}$$

$$+ \sum_{n=1}^{\infty} A_n \frac{qN_n}{nv} \sinh[nv(d_{sc}-z)]\cos(nvx),$$

$$(0 \leqslant z \leqslant d_{sc}). \qquad (2)$$

The corresponding electric field is given by

$$E_x(x,z)=\sum_{n=1}^{\infty} qN_nA_n \;\; \sinh\,[n\nu(d_{sc}-z)]\sin(n\nu x) \quad (3a)$$

and

$$E_z(x,z)=\frac{-V_0\epsilon_{lc}+qN_0d_{lc}}{\epsilon_{lc}d_{sc}+\epsilon_{sc}d_{lc}}+\sum_{n=1}^{\infty} qN_nA_n$$
$$\times \cosh\,[n\nu(d_{sc}-z)]\cos(n\nu x), \quad (3b)$$

where

$$A_n=\frac{1}{\epsilon_{sc}\;\cosh\,(n\nu d_{sc})+\epsilon_{lc}\;\sinh\,(n\nu d_{sc})/\;\tanh\,(n\nu d_{lc})},$$
$$n=1,2,3,\dots \;. \quad (4)$$

V_0 is the applied voltage in the write period, and d_{sc}, d_{lc}, ϵ_{sc}, and ϵ_{lc} are thicknesses and dielectric constants of the semiconductor and LC layers, respectively. The parameter q is the electronic charge, and it is positive for holes and negative for electrons. Any dielectric anisotropy in the semiconductor and LC layers is neglected.

The slope of lines of the electric field, including the fringing field, is the ratio of the x component to the z component of the electric field. Because the carriers follow the field lines, the effect of fringing fields or drift in the bulk, on resolution is independent of the carrier mobility in the semiconductor. From Eqs. (3) and (4) we can see that $E_z(x,z)$ is relatively constant with position x if the relative spatial variation in the interface charge $N(x)$, N_n/N_0 for all n, is much smaller than one. On the other hand, the amplitude of $E_x(x,z)$ increases with spatial frequency, and saturates when the spatial frequency is so high that $\nu>$minimum of $(2\pi/d_{sc},2\pi/d_{lc})$. The amplitude of $E_x(x,z)$ also increases with decreasing the distance z, and reaches its maximum value at the interface:

$$E_x(x,z=0)=\sum_{n=1}^{\infty} \frac{qN_n\,\sin\,(n\nu x)}{\epsilon_{sc}\;\coth\,(n\nu d_{sc})+\epsilon_{lc}\;\coth\,(n\nu d_{lc})}. \quad (5)$$

Thus the effect of fringing field on resolution increases with spatial frequency, and saturates when the spatial frequency is very high. The fringing field effect is most significant near the interface.

The electric field lines $z(x)$ can be found from integrating the following equation

$$\frac{dz(x)}{dx}=\frac{E_z(x,z)}{E_x(x,z)}. \quad (6)$$

The result is given by

$$\sum_{n=1}^{\infty} A_n\,\frac{qN_n}{n\nu}\{\cosh\,[n\nu(d_{sc}-z)]\sin(n\nu x)$$
$$-\cosh\,[n\nu(d_{sc}-z_0)]\sin(n\nu x_0)\}+A_0(x-x_0)=0 \quad (7)$$

where

$$A_0=\frac{-V_0\epsilon_{lc}+qN_0d_{lc}}{\epsilon_{lc}d_{sc}+\epsilon_{sc}d_{lc}}. \quad (8)$$
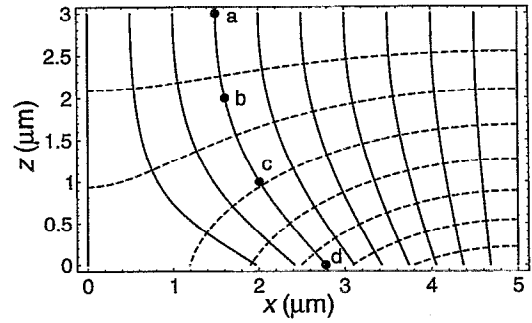

FIG. 2. Calculated electric field (continuous) and equipotential (dashed) lines in the semiconductor region created by a sinusoidal interface charge. The thicknesses of the semiconductor and liquid crystal layers are $d_{sc}=3$ μm and $d_{lc}=1$ μm, respectively, and the respective dielectric constants are $\epsilon_{sc}=12\epsilon_0$ and $\epsilon_{lc}=4\epsilon_0$, where ϵ_0 is the permittivity of free space. The applied voltage is 10 V, and the average and the first Fourier harmonic of the charge density at the interface are $N_0=0$ and $N_1=30$ nC/cm^2, respectively.

In Eq. (7) (x_0,z_0) is a point on a specific electric field line and (x,z) is a corresponding point along the same line. Figure 2 shows the electric field and equipotential lines in the semiconductor layer that are built up by a sinusoidal interface charge distribution. Charge carriers generated at point a drift to point d through points b and c under the electric field.

Figure 3 shows the effect of fringing fields on the final interface charge distribution, in which small modulation
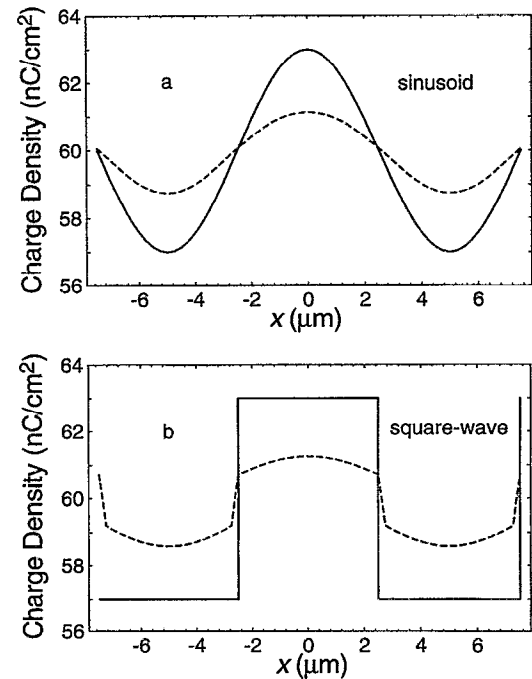

FIG. 3. Effect of fringing fields on distribution of photo-generated charge carriers at the interface resulting from a sinusoidal (a) and a square-wave (b) input pattern. Shown are the distributions with (dashed line) and without (continuous line) this effect. The initial charge density at the interface is uniform and equal to -35.4 nC/cm^2, which corresponds to no electric field in the liquid crystal. The applied voltage, geometric parameters, and the dielectric constants are the same as those of Fig. 2.
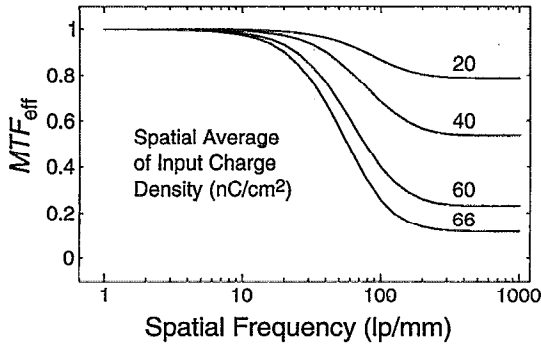
FIG. 4. Numerically determined effective modulation transfer function MTF_{eff} from input to final interface charge distribution resulting from charge drift in response to fringing fields. The modulation in the sinusoidal input charge is 1% for all the curves. Spatial average of input charge density for each curve is shown in the figure. The initial charge density at the interface is -35.4 nC/cm^2. The applied voltage, geometric parameters, and dielectric constants are the same as those of Fig. 2.

FIG. 5. Numerically deduced effective modulation transfer function MTF_{eff} from input to final interface charge distributions resulting from charge drift in response to fringing fields. The thicknesses of the semiconductor and the liquid crystal layers are $d_{sc}=25$ μm and $d_{lc}=4$ μm, respectively. The dielectric constants are the same as those of Fig. 2. The modulation in the sinusoidal input charge is 1% for all the curves. The spatial average of input charge density for each curve is shown in the figure. The initial charge density at the interface is 0. The applied voltage is 20 V.

(5%) and contrast ratio (5%) are used for both the sinusoidal and square-wave input charges. Although the reduction in modulation is evident in Fig. 3(a), the distortion in the resulting charge distribution is hard to discern. The distortion is apparent in Fig. 3(b), where the sharp corners are somewhat rounded off due to larger fringing field effects at higher spatial frequencies.

Figure 4 shows the MTF_{eff} curves with spatial frequency for various input charge densities. The MTF_{eff} decreases with spatial frequency. This is due to larger lateral electric fields at higher spatial frequencies that move more charge carriers from regions of high concentration to regions of low concentration. The fringing field effect saturates at very high frequencies. The MTF_{eff} also decreases with increasing total input charge. This is because as the total interface charge increases the vertical (i.e., normal to the interface) electric field $E_z(x,z)$ in semiconductor region is reduced and the relative effect of fringing field becomes larger. Thus it is expected that when the overall interface charge density is close to the saturation value (the interface charge density at which the electric field in the semiconductor becomes zero, equal to 70.8 nC/cm^2 in Fig. 4) its spatial variation along the interface may become so small that output image modulation is reduced significantly.

Figure 5 shows the MTF_{eff} curves for a device in which the semiconductor and LC layers are thicker than those of Fig. 4. It can be seen that the spatial resolution starts to decrease at significantly lower frequencies than in Fig. 4. As is shown in the first term in Eq. (3b) the vertical electric field $E_z(x,z)$ in semiconductor region decreases with thickness of the semiconductor and LC layers. Thus the relative effect of fringing fields is larger in a thicker device. To prevent this effect some devices with thick semiconductor layers are pixelated at the interface in an effort to preserve the spatial resolution by changing the electric field and impeding charge spreading in the semiconductor.[1,3,18,22] It is interesting to note that the measured resolutions in these patterned devices are far below the limiting resolutions defined by the pixel sizes. Either the confining effect is not efficient or other
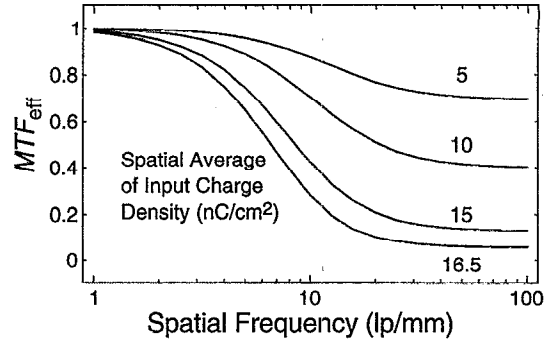
charge spreading processes determine the resolution. It is difficult to calculate or simulate the electric field distribution in these patterned devices due to the complicated interface charge distribution.

IV. BULK DIFFUSION EFFECT

The other important charge transport process in bulk region involves diffusion and recombination of charge carriers. It is described by the current continuity or rate equations.[23,24] Since we consider the semiconductor region to be homogeneous along the z direction the rate equations can be integrated over the whole thickness of the semiconductor layer excluding the semiconductor-LC interface. Ignoring the intrinsic carrier concentration and the thermal generation in the semiconductor, the sheet concentration of photo-generated charge carriers in transit $N_{trans}(x,t)$ at any time is given by

$$\frac{\partial N_{trans}(x,t)}{\partial t} = D_{\parallel} \frac{\partial^2 N_{trans}(x,t)}{\partial x^2} + g(x,t) - \frac{N_{trans}(x,t)}{\tau_r}$$

$$- \frac{N_{trans}(x,t)}{T_{trans}}, \qquad (9)$$

where $D_{\parallel}$ is the lateral diffusion coefficient in bulk region, $g(x,t)$ is the charge carrier generation rate from the incident photons in units of cm^{-2} s^{-1}, τ_r is the recombination lifetime in the bulk semiconductor, and parameter T_{trans} is the average transit time. The transit time depends on the electric field in the semiconductor and it varies with time and position in the write period. This variation produces an effect in Eq. (9) that is small compared with that of other temporal and spatial parameters in the rate equation, so to a first order approximation it can be treated as a constant. The last term in Eq. (9) is due to the charge accumulation at the interface. Since only those charge carriers that arrive at the interface contribute to the electric field and voltage modulation across the LC, the last term can be considered to be a charge collection rate defined as $g_{coll}(x,t) = N_{trans}(x,t)/T_{trans}$. This simplified diffusion process does not explicitly involve geometric param-

eters in the device structure so its results can be applied directly to unpatterned MQW modulators. Since the semiconductor region in the MQW modulators is not homogeneous, an average lateral diffusion coefficient must be used instead.

Consider a charge generation rate $g(x,t)$ such that

$$g(x,t) = \begin{cases} 0, & t \leq 0 \\ g_0[1 + m_{in} \cos(\nu x)], & t > 0 \end{cases}$$ (10)

where m_{in} is the modulation of the input charge. The analytical solution to Eq. (9) is given by

$$N_{trans}(x,t) = g_0\{\tau_0[1 - \exp(-t/\tau_0)] + m_{in}\tau_1[1 - \exp(-t/\tau_1)]\cos(\nu x)\},$$ (11)

where the effective carrier lifetime τ_0 is defined by

$$\frac{1}{\tau_0} \equiv \frac{1}{\tau_r} + \frac{1}{T_{trans}}$$ (12a)

and

$$\tau_1 = \frac{\tau_0}{1 + D_{\parallel}\tau_0\nu^2}.$$ (12b)

Usually the write time t needs to be much longer than the transit time T_{trans} to give any useful modulation in the output image, so Eq. (11) can be simplified to

$$N_{trans}(x,t) = g_0\tau_0\left(1 + m_{in}\frac{\tau_1}{\tau_0}\cos(\nu x)\right), \quad t \gg T_{trans}$$ (13)

and the charge collection rate $g_{coll}(x,t)$ becomes

$$g_{coll}(x,t) = g_0\frac{\tau_0}{T_{trans}}\left(1 + \frac{\tau_1}{\tau_0}m_{in}\cos(\nu x)\right).$$ (14)

Comparing this with the generation rate of photo-generated charge carriers in the bulk semiconductor in Eq. (10) we can see that both the spatial average and amplitude of $g_{coll}(x,t)$ are less than those of $g(x,t)$. This is due to charge recombination and diffusion in the bulk region. Some photo-generated charge carriers recombine before they arrive at the interface. This charge loss mechanism during transit can be characterized by a transport efficiency defined as the ratio of the spatial average of $g_{coll}(x,t)$ to that of $g(x,t)$ and given by $\eta = \tau_r/(\tau_r + T_{trans})$. If the recombination lifetime is much longer than the transit time then there is essentially no charge loss in bulk region, and almost all the photo-generated charge carriers arrive at the interface before they are recombined. The maximum sensitivity of the device depends upon the charge transport. When the recombination lifetime decreases, the transport efficiency also decreases. Increasing the concentration of defect states in the semiconductor layer can reduce the lifetime. As the incident write light continues to produce photo-generated carriers in the semiconductor during the write period the electric field in the semiconductor is reduced gradually and the transit time is increased, which also decreases the efficiency. The device is expected to be less sensitive at the end of write period than it is at the beginning. In terms of sensitivity it is favorable to operate the device with a high electric field in order to have

a short transit time. In some semi-insulating MQW modulators deep states are created on purpose to reduce the lateral mobility.[5,25] This is helpful in reducing lateral diffusion in the bulk region to preserve the spatial resolution (as is discussed in next paragraph). However, it also reduces the transport efficiency and sensitivity because of an increase in the transit time and a decrease in the recombination lifetime.

In addition to affecting the sensitivity, charge diffusion also reduces the modulation of the charge collection rate at the interface. The MTF for this charge spreading process can be calculated from Eqs. (10) and (14) and is given by

$$MTF = \frac{\tau_1}{\tau_0} = \frac{1}{1 + D_{\parallel}\tau_0\nu^2}.$$ (15)

The spatial frequency at which MTF decreases to 50% is $f_{50\%} = 1/(2\pi L_d)$, where $L_d = \sqrt{D_{\parallel}\tau_0}$ may be considered as an effective diffusion length for charge carriers in the bulk region. To reduce the bulk diffusion effect on resolution, the diffusion length L_d must be made as small as possible. Thus small values of τ_0 yield high resolutions. When the recombination lifetime τ_r is much shorter than the transit time T_{trans}, then $\tau_0 = \tau_r$ and L_d is just the usual carrier diffusion length. Short lifetimes reduce the diffusion length, but also reduce the transport efficiency η and sensitivity. On the other hand, if the recombination lifetime is much longer than the transit time, then $\tau_0 = T_{trans}$ and L_d becomes the length that the carriers diffuse during their transit. The transit time is $T_{trans} = d_{sc}^2/(\mu_{\perp}V_{sc})$, where d_{sc} is the thickness of the semiconductor layer, V_{sc} is the voltage across the semiconductor layer, and $\mu_{\perp}$ is the vertical mobility in the semiconductor. The diffusion length is given by

$$L_d = \sqrt{\frac{\mu_{\parallel}}{\mu_{\perp}}\frac{kT}{|q|V_{sc}}}d_{sc}, \quad \tau_r \gg T_{trans},$$ (16)

where k is the Boltzmann's constant, T is the absolute temperature, and the mobility $\mu_{\parallel}$ is obtained from the diffusion coefficient $D_{\parallel}$ through the Einstein relationship. The corresponding spatial frequency $f_{50\%}$ is equal to

$$f_{50\%} = \sqrt{\frac{\mu_{\perp}}{\mu_{\parallel}}}\sqrt{\frac{293.9}{T(K)}}\frac{\sqrt{V_{sc}(V)}}{d_{sc}}.$$ (17)

In this case the transport efficiency is unity, but the spatial resolution is poor if the semiconductor layer is very thick or V_{sc} is very small. Increasing the applied voltage can improve resolution of the device and its diffraction efficiency by reducing carrier transit or escape time to the semiconductor-dielectric interface.[26] The other way of preserving resolution is to reduce the lateral mobility $\mu_{\parallel}$ without changing the vertical mobility $\mu_{\perp}$. Otherwise lower vertical mobilities result in longer transit times and the transport efficiency decreases.

Figure 6 shows the spatial frequencies $f_{50\%}$ for various values of lateral mobility and the effective lifetime τ_0. Mobilities of charge carriers (usually electrons) in a-Si:H are very small (0.1–1.0 cm^2/V s), but the carrier lifetimes or transit times are relatively long. Photosensors of a-Si:H that are used in OASLMs are located at the upper right corner of this chart, indicating that the bulk diffusion process gives relatively high resolution (>100 1p/mm). Photosensors of
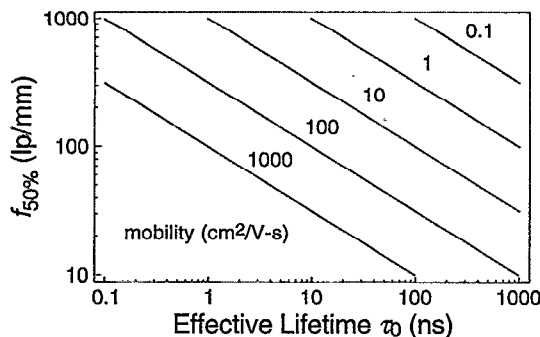
L. Wang and G. Moddel

FIG. 6. Effect of bulk diffusion on OASLM resolution. The spatial frequencies at which the MTF decreases to 50% are plotted versus the effective lifetime τ_0. The lateral mobility for each curve is shown in the figure.

crystalline semiconductors such as GaAs, AlGaAs, and Si that are used in MQW modulators and other OASLMs have very high lateral mobilities (100–3000 cm^2/V s). However, their very short recombination lifetime and/or transit time result in a relatively small diffusion length L_d that puts them at the upper left corner of this chart, indicating that their bulk diffusion process also results in high resolution (>100 lp/mm). Thus the effect of bulk diffusion on resolution is largely independent of the mobility in the bulk of the semiconductor. Since the measured resolution (i.e., spatial frequency at which the MTF decreases to 50%) in most OASLMs is much lower than 100 lp/mm, the resolution of the OASLMs is limited mainly by other transfer processes in these devices, and the bulk diffusion effect is negligible in most cases.

V. CHARGE SPREADING AT INTERFACE

In Secs. III and IV we have discussed the effects that both fringing fields and diffusion in the bulk region have in reducing the modulation depth of charge accumulating at the interface. Once the charge carriers arrive at the interface they diffuse and drift laterally until they are trapped or the write period ends. This charge spreading by drift and diffusion further reduces the modulation depth in final charge distribution. The interface properties have a strong influence on this transport process. A defect-free interface allows charge carriers to diffuse and drift a great distance. An interface with many defects may trap carriers as soon as they arrive, which helps to preserve spatial resolution. There are several factors contributing to the trapping process, including defect states at the interface and coulombic attraction from induced opposite-sign charge (e.g., spontaneous polarization in ferroelectric LC). The trapping time τ_t can be written generally in terms of a trapping time τ_{ti} for each individual trapping process

$$\frac{1}{\tau_t} = \sum_i \frac{1}{\tau_{ti}}. \tag{18}$$

In all following discussions only τ_t, and hence only the combined effect of these trapping processes, is considered. Because of the vertically applied electric field there are no free opposite-sign charge carriers at the interface, so that no re-

combination occurs during this interface transport process. It is assumed in the analysis that the charge carriers deposited at the interface are released and/or recombined with the opposite-sign charge carriers during the following reset period.

Rate equations describing diffusion, drift, and trapping at the interface are similar to Eq. (9) and are given by

$$\frac{\partial N_{\text{free}}(x,t)}{\partial t} = -\frac{1}{q}\frac{\partial J_{\text{free}}(x,t)}{\partial x} + G_{\text{coll}}(x,t) - \frac{N_{\text{free}}(x,t)}{\tau_t} \tag{19a}$$

and

$$\frac{\partial N_{\text{trap}}(x,t)}{\partial t} = \frac{N_{\text{free}}(x,t)}{\tau_t}, \tag{19b}$$

where $N_{\text{free}}(x,t)$ and $N_{\text{trap}}(x,t)$ are the free and trapped charge concentrations accumulated at the interface, and $G_{\text{coll}}(x,t)$ is the carrier collection rate at the interface. The magnitude of $G_{\text{coll}}(x,t)$ varies with time and position, and is determined by both the drift and diffusion processes in the bulk region. It is clear from discussions in Secs. III and IV that no analytic form can be found for $G_{\text{coll}}(x,t)$ even though the photo-generated charge may have a simple, sinusoidal distribution. This is due to the inherent nonlinearity in the charge drift process. In order to investigate the effect of charge spreading at the interface on the spatial resolution, $G_{\text{coll}}(x,t)$ will be assumed to be constant with time t. $J_{\text{free}}(x,t)$ in Eq. (19a) is the sheet current density resulting from diffusion and drift of free charge carriers at the interface, and is given by[23,24]

$$J_{\text{free}}(x,t) = |q|\mu_s E_x(x,t)N_{\text{free}}(x,t) - qD_s\frac{\partial N_{\text{free}}(x,t)}{\partial x}, \tag{20}$$

where $E_x(x,t)$ is the lateral electric field at the interface given by Eq. (5), D_s and μ_s are diffusion coefficient and mobility of carriers at the interface, which may be different from those in bulk region.

If the distributions of free and trapped interface charge carriers have the following forms

$$N_{\text{free}}(x,t) = N_{f0}(t) + \sum_{n=1}^{\infty} N_{fn}(t)\cos(n\nu x) \tag{21a}$$

and

$$N_{\text{trap}}(x,t) = N_{t0}(t) + \sum_{n=1}^{\infty} N_{tn}(t)\cos(n\nu x), \tag{21b}$$

then $E_x(x,t)$ becomes

$$E_x(x,t) = \sum_{n=1}^{\infty} \frac{q[N_{fn}(t)+N_{tn}(t)]\sin(n\nu x)}{\epsilon_{sc}\ \coth\ (n\nu d_{sc}) + \epsilon_{lc}\ \coth\ (n\nu d_{lc})}. \tag{22}$$

By substituting the current density $J_{\text{free}}(x,t)$ into Eq. (19a) we get a nonlinear partial differential equation for the free charge carrier concentration

$$\frac{\partial N_{\text{free}}(x,t)}{\partial t} = \pm \mu_s E_x(x,t) \frac{\partial N_{\text{free}}(x,t)}{\partial x}$$

$$\pm \mu_s \frac{\partial E_x(x,t)}{\partial x} N_{\text{free}}(x,t) + D_s \frac{\partial^2 N_{\text{free}}(x,t)}{\partial x^2}$$

$$+ G_{\text{coll}}(x,t) - \frac{N_{\text{free}}(x,t)}{\tau_t}. \tag{23}$$

The minus signs in front of the first two terms on the right-hand side of Eq. (23) are for holes, and the plus signs for electrons. Equation (23) can also be applied to unpatterned three-layer MQW modulators as long as these devices exhibit a symmetry both in structure and in charge distribution that is described in Appendix B. Since the lateral electric field is independent of the vertically applied voltage and of the initial (at time $t=0$) uniform charge trapped at the interface, this charge spreading process does not involve these two parameters.

One common way to simplify Eq. (23) is to assume a sinusoidal charge collection pattern and neglect higher-order harmonics in free and trapped carrier distributions, and apply a small-modulation approximation. Unfortunately the resulting equations do not converge in time t due to the inherent nonlinearity in this charge transport process. We can gain some insights into this nonlinearity by inspecting Eqs. (20) and (22). The diffusion current in Eq. (20) is proportional only to the spatially varying part of the free charge at the interface. The drift current is proportional not only to the spatially varying part of total interface charge in $E_x(x,t)$ but also to the magnitude of the free charge. Thus we can think of the sheet current as a diffusion current having two different diffusion coefficients. One of these is just the normal diffusion constant and the other is a pseudo-constant which is proportional to the magnitude of the free interface charge. This pseudo-diffusion coefficient neither vanishes nor becomes constant when the charge modulation amplitude approaches zero, and the nonlinearity due to it does not vanish unless the interface charge is zero.

Using a numerical approach is a good way to solve Eq. (23). We choose the Crank–Nicolson implicit method that gives convergent and stable solutions most of the time.[27,28]

A. Diffusion effect at interface

We examine the diffusion effect analytically before proceeding to the full numerical solution. Although the analysis is less accurate than the numerical solution, these simple, analytical results do give us some insights into charge spreading at the interface. The effect of charge drift, due to the lateral electric field, is to accelerate the charge spreading process at the interface.

One of the devices that this approximation can be applied to is the OASLM incorporating surface stabilized ferroelectric LCs (SSFLCs).[2,20] the SSFLC exhibits macroscopic ferroelectricity, which results in charge at its surface. When the SSFLC layer switches from one stable state to the other, the total amount of charge needed is $2P$, where P is the ferroelectric polarization. In these devices many of the photogenerated charge carriers that arrive at the interface may be compensated for by the opposite-sign surface charge of the SSFLC layer. Thus there is reduced net spatial charge variation and therefore a reduced lateral electric field exists at the interface. In this case the fringing field effect is also reduced.

When the lateral electric field is neglected, Eq. (23) becomes

$$\frac{\partial N_{\text{free}}(x,t)}{\partial t} = D_s \frac{\partial^2 N_{\text{free}}(x,t)}{\partial x^2} + G_{\text{coll}}(x,t) - \frac{N_{\text{free}}(x,t)}{\tau_t}. \tag{24}$$

As does Eq. (9), Eq. (24) describes a linear process, and the effect of this process on resolution can be fully characterized by the MTF. Suppose the carrier collection rate $G_{\text{coll}}(x,t)$ has the following form

$$G_{\text{coll}}(x,t) = \begin{cases} 0, & t \leq 0 \\ G_0[1 + M_{\text{in}} \cos(\nu x)], & t > 0, \end{cases} \tag{25}$$

where M_{in} is the modulation and G_0 is the spatial average of the charge collection rate. The analytical solution to Eq. (24) is given by

$$N_{\text{free}}(x,t) = G_0\{\tau_t[1 - \exp(-t/\tau_t)]$$

$$+ M_{\text{in}}\tau_2[1 - \exp(-t/\tau_2)]\cos(\nu x)\}, \tag{26a}$$

where $\tau_2 = \tau_t/(1 + D_s\tau_t\nu^2)$. The trapped carrier concentration of Eq. (19b) becomes

$$N_{\text{trap}}(x,t) = G_0\{t - \tau_t[1 - \exp(-t/\tau_t)]\} + M_{\text{in}}G_0$$

$$\times \frac{\tau_2}{\tau_t}\{t - \tau_2[1 - \exp(-t/\tau_2)]\}\cos(\nu x). \tag{26b}$$

For an interface with many defects, the trapping time τ_t can be much shorter than the write time t. Charge carriers coming from the bulk region are trapped as soon as they arrive at the interface. In this case free and trapped carrier concentrations in Eq. (26) are given by

$$N_{\text{free}}(x,t) = G_0\tau_t\left(1 + M_{\text{in}}\frac{\tau_2}{\tau_t}\cos(\nu x)\right), \quad t \gg \tau_t \tag{27a}$$

and

$$N_{\text{trap}}(x,t) = G_0 t\left(1 + M_{\text{in}}\frac{\tau_2}{\tau_t}\cos(\nu x)\right), \quad t \gg \tau_t. \tag{27b}$$

It can be seen from Eq. (27) that the vast majority of the photo-generated carriers collected at the interface are trapped at time t. The MTF for this process is the ratio of the modulation of the total carrier concentration to that of the charge collection rate, and is given by

$$\text{MTF} = \frac{\tau_2}{\tau_t} = \frac{1}{1 + D_s\tau_t\nu^2}. \tag{28}$$

It has exactly the same form as Eq. (15) except that the lateral diffusion coefficient in bulk and the time constant τ_0 are replaced by the diffusion coefficient and the trapping time at the interface, respectively. Thus the discussions in Sec. IV can be applied to the interface diffusion process, and it is clear that short trapping times and low mobilities at the interface help preserve high spatial resolutions. In contrast to the bulk diffusion effect, the interface diffusion effect does

L. Wang and G. Moddel

not affect the charge transport efficiency. Reducing the mobility and the trapping time at the interface improves the resolution of the OASLMs as long as the trapped charge at the interface can be completely released and/or recombined with opposite-sign charge carriers during the following reset period. If this reset process were impeded, residual charge images created in previous write periods would affect the addressing of the device in the following write periods. In some semi-insulating MQW modulators the interfacial layer between the MQW region and the dielectric layer is grown at lower temperatures in an effort to reduce this diffusion effect.[5,6]

If the interface is free from any trapping defects, then the trapping time may be much longer than the write period. In this case the last term in Eq. (24) is negligible and essentially no trapped charge carriers exist at the interface. The solution to Eq. (24) becomes

$$N_{\text{free}}(x,t)$$
$$= G_0 t \left(1 + M_{\text{in}} \frac{1 - \exp(-D_s \nu^2 t)}{D_s \nu^2 t} \cos(\nu x) \right),$$
$$t \ll \tau_t. \tag{29}$$

The MTF for this process is given by

$$\text{MTF} = \frac{1 - \exp(-D_s \nu^2 t)}{D_s \nu^2 t}. \tag{30}$$

It decreases with time significantly when $t > 1/(D_s \nu^2)$. The spatial frequency $f_{50\%}$ at which the MTF decreases to 50% at the end of the write period t_{write} is $f_{50\%} = 1.26/(2\pi\sqrt{D_s t_{\text{write}}})$, where $\sqrt{D_s t_{\text{write}}}$ is the distance that the free charge carriers diffuse along the interface during the write period. Preserving the spatial resolution in this particular case requires that the write period must be short enough so that the diffusion length of the charge carriers at the interface $\sqrt{D_s t_{\text{write}}}$ is smaller than the smallest features in the input light beam.

B. Complete numerical solution

The simple calculation in Sec. V A accounts only for the diffusion effect, and the result is suitable only for some specific devices. In general, a lateral electric field also exists at the interface because of charge nonuniformity. Charge carriers drift under this electric field and the spatial charge modulation is reduced further. There are many parameters involved in this charge spreading process which include mobility, trapping time at the interface, and geometric and electro-static parameters for the device. The device may be operated with various applied voltages and frequencies. Instead of trying to cover and discuss the whole range of combinations for these parameters and driving conditions, some typical device structures and parameters are used to illustrate the charge spreading effects at the interface.

Figure 7 shows the photo-generated charge distribution at the interface at the end of write period. The figure includes the results from both diffusion alone and the numerical solution of Eq. (23) that accounts for diffusion and drift. The effect of diffusion appears only in regions where the charge
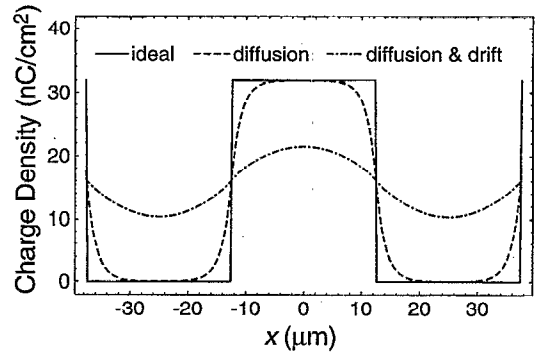

FIG. 7. Calculated interface charge distributions at the end of write period due to diffusion and drift at interface. Shown are the ideal case without diffusion and drift (continuous line), the effect of diffusion (dashed line), and the effects of diffusion and drift (dash-dotted line). The geometric parameters and dielectric constants are the same as those of Fig. 2. The write time, the trapping time, and the mobility at the interface are 0.5 ms, 1 μs, and 1 cm^2/V s, respectively. The charge collection rate is a square-wave having a spatial average of 2×10^{14}/cm^2 s and a contrast ratio of 1.

collection rate varies rapidly with position. It does not affect the overall shape of the resulting charge distribution and its contrast ratio. On the other hand, when charge drift is present, the charge distribution at this spatial frequency is distorted more significantly. The contrast ratio of the final charge distribution, which is determined mainly by the amplitude of the fundamental harmonic, is reduced by the large drift effect. This drift effect is more severe at higher spatial frequencies, so that any charge modulations in higher-order harmonics are eliminated almost completely, which results in a sinusoid-like charge distribution.

Figure 8 shows the dependence of the MTF$_{\text{eff}}$ on the modulation and the magnitude of the sinusoidal charge collection rate. Just as is shown in Fig. 7, the effects of charge spreading on the values of MTF$_{\text{eff}}$ and the effective modulation in the final charge distribution increase with spatial frequency. These effects also increase with increasing magni-
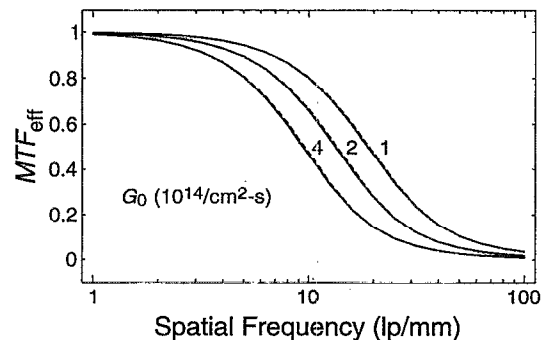

FIG. 8. Numerically deduced effective modulation transfer function MTF$_{\text{eff}}$ from a charge collection pattern to the final interface charge distribution due to the diffusion and drift at the interface. The geometric parameters and dielectric constants are the same as those of Fig. 2. The write time, trapping time, and the mobility at the interface are the same as those of Fig. 7. The charge collection rate $G_{\text{coll}}(x,t)$ is sinusoidal, and its spatial average G_0 for each curve is shown in the figure. The modulation of the charge collection rate is 0.1 (continuous line) and 1 (dashed line), respectively.
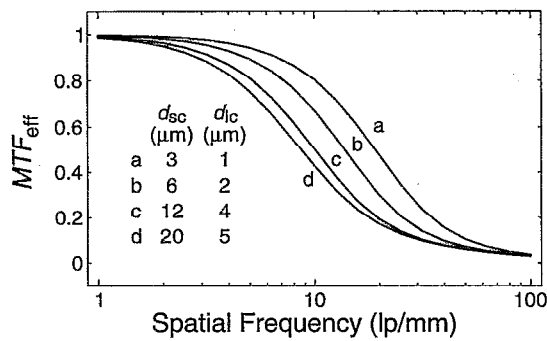
FIG. 9. Numerically deduced effective modulation transfer function $\mathrm{MTF_{eff}}$ from a charge collection pattern to the final interface charge distribution due to diffusion and drift at the interface. The thicknesses of the semiconductor and liquid crystal layers for each curve are shown in the figure. The dielectric constants are the same as those of Fig. 2. The write time, trapping time, and the mobility at the interface are the same as those of Fig. 7. The charge collection rate $G_{coll}(x,t)$ is sinusoidal and has a spatial average of $1 \times 10^{14}/\mathrm{cm}^2$ s and a modulation of 1.

FIG. 10. Numerically deduced effective modulation transfer function $\mathrm{MTF_{eff}}$ from a charge collection pattern to the final interface charge distribution due to diffusion and drift at the interface. The geometric parameters and dielectric constants are the same as those of Fig. 2. The write time is 0.5 ms. The diffusion length at the interface for each curve is shown in the figure. The charge collection rate $G_{coll}(x,t)$ is sinusoidal and has a spatial average of $1 \times 10^{14}/\mathrm{cm}^2$ s and a modulation of 1.

tude of the charge collection rate. This is due to the larger pseudo diffusion coefficients that have been discussed at the beginning of Sec. V. We note that in Fig. 8 the variation of the modulation in the charge collection rates barely changes the values of $\mathrm{MTF_{eff}}$.

From Eq. (22) we can see that the lateral electric field at the interface increases with the thickness of semiconductor or LC layer, so that it is expected that effects of charge spreading on resolution are more significant in OASLMs with thicker semiconductor or LC layers. The numerically-deduced $\mathrm{MTF_{eff}}$ curves for OASLMs having several thicknesses of semiconductor and liquid crystal layers are shown in Fig. 9. The spatial frequency at which the $\mathrm{MTF_{eff}}$ decreases to 50% is reduced from 19.1 lp/mm to 8.6 lp/mm when the thicknesses of the respective semiconductor and LC layers increase from 3 and 1 μm to 20 and 5 μm.

Mobility and trapping time are the two most significant parameters characterizing the interface. Free charge carriers having lower mobilities or shorter trapping times at the interface have less chance or time to diffuse and drift before they are trapped by the defect states. In the numerical solutions of Eq. (23) we have found that interfaces having the same diffusion length $\sqrt{D_s t_t}$ give virtually the same $\mathrm{MTF_{eff}}$. Quite similar $\mathrm{MTF_{eff}}$ curves are also obtained as long as the total amount of collected charge, which is the product of the charge collection rate and the writing time, remains constant and the trapping time is much shorter than the writing time. Figure 10 shows the calculated $\mathrm{MTF_{eff}}$ as a function of spatial frequency for various values of diffusion length $\sqrt{D_s t_t}$. Decreasing the mobility or the trapping time at the interface, which reduces the diffusion length, can dramatically improve the resolution of OASLMs. The spatial frequency $f_{50\%}$ increases from 3.04 to 875 lp/mm when the diffusion length is reduced from 10 to 0.1 μm. Without including drift the increase is from 15.9 to 1590 lp/mm.
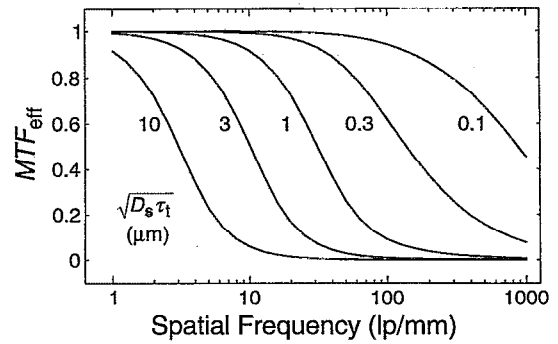
VI. DISCUSSION AND CONCLUSIONS

The possible transfer processes from the input image to the output image in an OASLM are summarized in Fig. 11. The resolution of the OASLM may be degraded during each of these transfer processes. It has been shown in the previous sections that during the transfer process from the input image to the interface charge effects of fringing fields, charge diffusion in the bulk, and charge drift and diffusion at the interface reduce the resolution of OASLMs. The resolution of OASLMs decreases further when the interface charge is converted to the electric field or voltage in the light-modulating layer, which is characterized by a charge-to-voltage MTF:[12,18]

$$\mathrm{MTF}_{c \to v} = \frac{\epsilon_{lc}/d_{lc} + \epsilon_{sc}/d_{sc}}{\nu[\epsilon_{lc} \coth(\nu d_{lc}) + \epsilon_{sc} \coth(\nu d_{sc})]}. \quad (31)$$

The final resolution-degrading mechanism results from the transfer process from voltage to the output image. This modulation of the output light beam by the electric field or
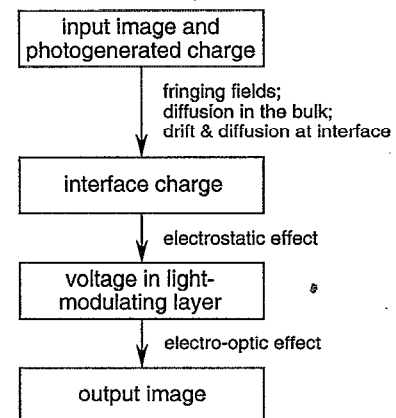

FIG. 11. Resolution-degrading mechanisms in an optically addressed spatial light modulator during the transfer processes from the input image to the output image.

TABLE I. Spatial frequencies $f_{50\%}$ and $f_{10\%}$ at which the MTF or the MTF_{eff} of each of the charge-to-voltage transfer process, the effect of bulk diffusion, and the effect of charge spreading at interface decreases to 50% and 10%, respectively. Also listed are $f_{50\%}$ and $f_{10\%}$ that correspond to the MTF of the OASLM. The MTF of the OASLM is deduced by taking the product of the MTF or the MTF_{eff} of each resolution-degrading mechanism. The applied voltage is 10 V for all the device structures. The writing time is 0.5 ms. The dielectric constants are $12\epsilon_0$ and $4\epsilon_0$ for the semiconductor and the LC layers, respectively, where ϵ_0 is the permittivity of free space. Modulation of 1% is assumed for both the fringing field effect and the charge spreading at the interface. Q_{init}: initial interface charge, N_0: spatial average of the photogenerated charge at the interface, G_0: spatial average of the charge collection rate, τ_0: the time constant defined by Eq. (12a), and is usually approximately the transit time.

	Charge-to-voltage transfer process		Bulk Diffusion			Diffusion and Drift at Interface			Resolution of OASLM	
	$f_{50\%}$	$f_{10\%}$	$\sqrt{D_{\parallel}\tau_0}$	$f_{50\%}$	$f_{10\%}$	$\sqrt{D_s\tau_t}$	$f_{50\%}$	$f_{10\%}$	$f_{50\%}$	$f_{10\%}$
	(lp/mm)		(μm)	(lp/mm)		(μm)	(lp/mm)		(lp/mm)	
$d_{sc}=3\,\mu$m, $d_{1c}=1\,\mu$m	144.7	812.3	0.5	318.3	954.9	0.1	307.6	1218	77.8	215.6
$Q_{\text{init}}=-35.4$ nC/cm^2						0.3	57.4	226.4	44.5	106.1
$N_0=30$ nC/cm^2						1	15.5	41.6	15.1	38.4
$G_0=3.75\times10^{14}$/cm^2 s						3	5.23	12.8	5.21	12.7
			1	159.2	477.5	0.1	307.6	1218	68.0	168.3
						0.3	57.4	226.4	42.5	97.1
						1	15.5	41.6	15.0	37.8
						3	5.23	12.8	5.21	12.7
			2	79.6	238.8	0.1	307.6	1218	51.7	120.8
						0.3	57.4	226.4	37.1	81.5
						1	15.5	41.6	14.7	35.9
						3	5.23	12.8	5.20	12.6
$d_{sc}=6\,\mu$m, $d_{1c}=2\,\mu$m	72.2	396.2	0.5	318.3	954.9	0.1	556.5	1359	47.2	165.2
$Q_{\text{init}}=-17.7$ nC/cm^2						0.3	74.3	421.8	35.2	93.4
$N_0=15$ nC/cm^2						1	15.9	47.5	14.5	36.6
$G_0=1.875\times10^{14}$/cm^2 s						3	5.24	13.0	5.17	12.6
			1	159.2	477.5	0.1	556.5	1359	44.3	127.6
						0.3	74.3	421.8	34.0	85.8
						1	15.9	47.5	14.4	36.0
						3	5.24	13.0	5.18	12.6
			2	79.6	238.8	0.1	556.5	1359	35.7	93.2
						0.3	74.3	421.8	30.6	72.6
						1	15.9	47.5	14.1	34.6
						3	5.24	13.0	5.17	12.5
$d_{sc}=12\,\mu$m, $d_{1c}=4\,\mu$m	36.8	210.4	0.5	318.3	954.9	0.1	925.2	1465	24.9	105.4
$Q_{\text{init}}=-8.85$ nC/cm^2						0.3	130.7	865	22.3	77.2
$N_0=7.5$ nC/cm^2						1	17.8	75.6	12.8	33.4
$G_0=9.375\times10^{13}$/cm^2 s						3	5.31	13.8	5.08	12.2
			1	159.2	477.5	0.1	925.2	1465	24.4	89.2
						0.3	130.7	865	21.9	71.0
						1	17.8	75.6	12.7	33.0
						3	5.31	13.8	5.08	12.2
			2	79.6	238.8	0.1	925.2	1465	22.7	69.2
						0.3	130.7	865	20.7	59.8
						1	17.8	75.6	12.5	31.6
						3	5.31	13.8	5.07	12.1

the voltage is a complicated process. It employs the Pockels effect or the linear electro-optic effect in light-modulating layers, quantum-confined Stark effect in MQWs, or highly nonlinear and time-dependent electro-optic effects in LCs. In most cases, however, the transfer processes of input image to the interface charge and to the voltage distributions are the most significant factors in determining the resolution of OASLMs. Although it is difficult to calculate accurately due to the nonlinear transfer processes in the device, the MTF of an OASLM may be expressed to a first-order approximation as the product of $\text{MTF}_{c \to v}$ and the MTF, or the MTF_{eff} of each of the charge spreading mechanisms described above.

Spatial frequencies at which each of the MTF and the MTF_{eff} decreases to 50% and 10%, $f_{50\%}$, and $f_{10\%}$, are calculated, and the result is listed in Table I. The result from the

fringing field effect is not listed since the calculated MTF_{eff} is greater than 50% at any spatial frequency, but it is used to calculate the MTF of the OASLM. From the table we can see that although the effect on resolution of the OASLM from each of the charge spreading mechanisms and the charge-to-voltage transfer process may be small, their combined effect is substantial. The corresponding $f_{50\%}$ of the OASLM is significantly smaller than that calculated for any of the resolution-degrading mechanisms. If the effect of one of the charge spreading mechanisms or the charge-to-voltage transfer process is much larger than that of the others, the resolution of the OASLM is largely determined by that resolution-degrading mechanism. Since the effects of the fringing field and charge spreading at the interface are charge-density dependent, the resolution of the OASLM is also a function of

charge density. The MTF of the OASLM can be obtained from the diffraction measurement which takes into account of the nonlinearity and the resolution of the device in a two-step model.[29]

The resolution of OASLMs can be improved only by reducing the effect of each of the resolution-degrading mechanisms. As with the charge-to-voltage transfer process, carrier drift due to the fringing field is a function of the thickness and dielectric constants of the semiconductor and the light-modulating layers, but is independent of the carrier mobility. If the resolution of an OASLM is limited mainly by the fringing field effect or the charge-to-voltage transfer process, the resolution may be improved by reducing the thickness of the semiconductor or the light-modulating layer. A very thin semiconductor, however, may be difficult to obtain (e.g., crystalline semiconductors such as Si and GaAs) or may reduce the sensitivity of the OASLM due to the decrease in the light absorption. The output light beam may not be sufficiently modulated by a very thin light-modulating layer, either. The fringing field effect increases with the total amount of photo-generated charge at the interface. This effect can be reduced by avoiding operation of the OASLM near the saturation regime.

The effect of bulk diffusion on resolution is less significant than that of other charge spreading mechanisms in OASLMs with both crystalline and amorphous semiconductor photosensors. Bulk diffusion is limited by the lateral distance that photo-generated charge carriers diffuse during transit, which is inversely proportional to the product of the mobility and the transit time. The transit time is inversely proportional to the mobility, however, so that the lateral diffusion distance is independent of bulk mobility to first order. The transit time and thus the effect of bulk diffusion on resolution can be reduced by decreasing the thickness of the semiconductor layer, or by increasing the applied voltage to the OASLM.

Charge spreading at the interface is often the most significant degrading mechanism in real devices. The resolution of an OASLM that has a defect-free interface is inversely proportional to the square root of the writing time τ_{write} (see Sec. V A and Ref. 20). In an OASLM that has many trapping defects at the interface, however, the resolution is largely independent of the writing time and becomes a strong function of the trapping time instead. To improve the resolution, the mobility and/or the trapping time of charge carriers at the interface can be reduced by such means as low-temperature growth of the interfacial semiconductor layer or ion implantation. It is worth warning, however, that the defect states introduced during the interface treatment might result in large excess dark or leakage current, and the following reset or erase period must be capable of removing the trapped charge. Otherwise, the performance of the OASLM will be severely affected by the formation of a residual image and by switching in the absence of a write light. If the charge spreading mechanisms are negligible in an OASLM without patterned pixels, then the degrading mechanisms in determining the resolution of the device are the thickness-dependent fringing field effect and the charge-to-voltage transfer process.
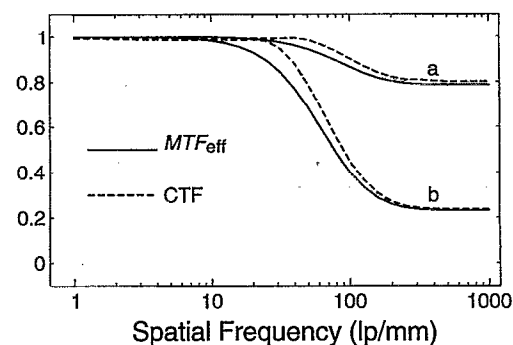

FIG. 12. Numerically deduced MTF$_{\text{eff}}$ and CTF from input to final interface charge distribution resulting from charge drift in response to fringing fields. The modulation for the sinusoidal input and the contrast ratio for the square-wave input are 1% for all the curves. Spatial average of input charge density is a: 20 nC/cm^2 and b: 60 nC/cm^2. The initial charge density at the interface is −35.4 nC/cm^2. The applied voltage, geometric parameters, and dielectric constants are the same as those of Fig. 2.

ACKNOWLEDGMENTS

APPENDIX A

In evaluating the spatial resolution characteristics in an optical system, an alternative to measuring the MTF in response to a sinusoidal input is the square-wave response test in which the contrast transfer properties to a square-wave target having various spatial frequencies are measured.[30] The contrast ratio of a target or an image is CR=$(I_{\text{max}} - I_{\text{min}})/(I_{\text{max}} + I_{\text{min}})$, where I_{max} and I_{min} are the respective local light-intensity maxima and minima on the target or image. The CTF may be defined as CTF=CR$_{\text{out}}$/CR$_{\text{in}}$, where CR$_{\text{out}}$ and CR$_{\text{in}}$ are the contrast ratios of the periodic output and input images, respectively. The CTF can also be used to characterize the effects of charge spreading on the resolution of an OASLM. Figure 12 shows the calculated CTF and the MTF$_{\text{eff}}$ due to the fringing field effect. These two functions are hardly distinguishable at both very low and very high spatial frequencies. Their difference is most significant at the intermediate frequencies.

APPENDIX B

A cross section of a symmetric PROM[11] or a three-layer MQW modulator[5] is shown in Fig. 13. When the write light is incident on the device, positive and negative charges are created at the two opposite semiconductor-dielectric interfaces by accumulation of photo-generated holes and electrons, respectively. Usually the magnitudes of the positive and negative charge are not equal to each other due to the different diffusion coefficients and mobilities for electrons and holes. To simplify the modeling and calculation, however, the charges are assumed to be equal to each other in magnitude in the write period,[11] i.e., $N(x,t)$ for the upper
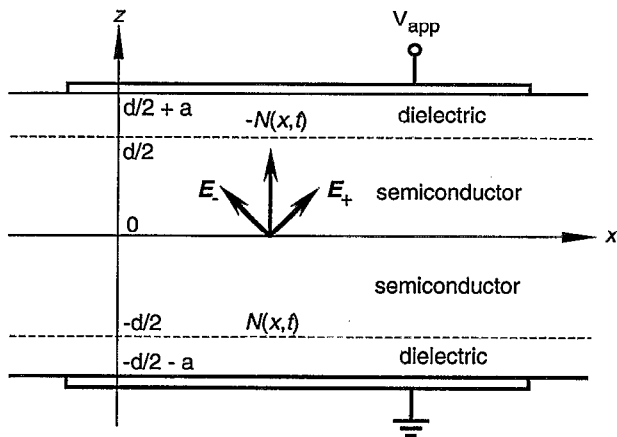
L. Wang and G. Moddel

FIG. 13. Schematic cross section of a symmetric PROM or multiple quantum well spatial light modulator. The charge distribution at the two semiconductor-dielectric interfaces is assumed to be equal in magnitude and have opposite signs. The thicknesses of the semiconductor and dielectric layers are d and a, respectively.

interface and $-N(x,t)$ for the lower interface. Consider the electric field at a point on the $z=0$ plane. The electric field created by the positive charge at the lower interface is assumed to be $\mathbf{E}_+$, and the electric field created by the negative charge at the upper interface, $\mathbf{E}_-$, is equal to $\mathbf{E}_+$ in magnitude. The total electric field created by the interface charge must be perpendicular to the $z=0$ plane due to the symmetry of the device structure about the $z=0$ plane. This is also true for the electric field resulting from the applied voltage V_{app}. Therefore the total electric field at any point on the $z=0$ plane is perpendicular to this plane. The $z=0$ plane becomes an equipotential plane and its electric potential is $V_{app}/2$. Comparing the bottom part ($z \leq 0$) of the device with the structure of LC OASLM in Fig. 1, it can be seen that both have exactly the same structure and boundary condition. Discussions in Sec. V can be applied to the symmetric PROM or MQW modulator if the thickness d_{sc} and d_{lc} are replaced with $d/2$ and a, respectively. Once the positive charge distribution at the lower semiconductor-dielectric interface is found, the negative charge distribution at the upper

semiconductor-dielectric interface is obtained immediately, as is the voltage distribution across the semiconductor layer.

[1] U. Efron, J. Grinberg, P. O. Braatz, M. J. Little, P. G. Reif, and R. N. Schwartz, J. Appl. Phys. 57, 1356 (1985).
[2] G. Moddel, K. M. Johnson, W. Li, R. A. Rice, L. A. Pagano-Stauffer, and M. A. Handschy, Appl. Phys. Lett. 55, 537 (1989).
[3] D. Armitage, J. I. Thackara, and W. D. Eades, Appl. Opt. 28, 4763 (1989).
[4] G. Moddel, Chap. 6 in Spatial Light Modulator Technology: Materials, Devices, and Applications, edited by U. Efron (Marcel Dekker, New York, 1994), pp. 287–359.
[5] A. Partovi, A. M. Glass, D. H. Olson, G. J. Zydzik, and H. M. O'Bryan, Appl. Phys. Lett. 62, 464 (1993).
[6] S. R. Bowman, W. S. Rabinovich, C. S. Kyono, D. S. Katzer, and K. Ikossi-Anastasiou, Appl. Phys. Lett. 65, 956 (1994).
[7] B. A. Horwitz and F. J. Corbett, Opt. Eng. 17, 353 (1978).
[8] Y. Nagao, H. Sakata, and Y. Mimura, Appl. Opt. 31, 3966 (1992).
[9] A. D. Fisher, Int. J. Optoelectron. 5, 125 (1990).
[10] J. Chen and T. Minemoto, J. Opt. Soc. Am. A 6, 1281 (1989).
[11] D. D. Nolte, Opt. Commun. 92, 199 (1992).
[12] W. R. Roach, IEEE Trans. Electron. Dev. ED-21, 453 (1974).
[13] Y. Owechko and A. R. Tanguay, Jr., J. Opt. Soc. Am. A 1, 635 (1984).
[14] S. S. Ignatosyan, Sov. J. Opt. Technol. 55, 198 (1988).
[15] Y. A. Flegontov, Sov. J. Opt. Technol. 60, 466 (1993).
[16] S. Fukushima, T. Kurokawa, and M. Ohno, Appl. Opt. 31, 6859 (1992).
[17] D. Williams, S. G. Latham, C. M. J. Powles, M. A. Powell, R. C. Chittick, A. P. Sparks, and N. Collings, J. Phys. D: Appl. Phys. 21, S156 (1988).
[18] D. Armitage, W. W. Anderson, and T. J. Karr, IEEE J. Quantum Electron. QE-21, 1241 (1985).
[19] P. B. Barbier and G. Moddel, Appl. Opt. 31, 3898 (1992).
[20] G. Moddel, Chap. 11 in Amorphous and Microcrystalline Semiconductor Devices: Optoelectronic Devices, edited by J. Kanicki (Artech House, Norwood, MA, 1991), pp. 369–412.
[21] W. J. Smith, in Handbook of Optics, edited by W. G. Driscoll and W. Vaughan (McGraw-Hill, New York, 1978), Sec. 2.
[22] M. C. Hebbron and S. S. Makh, SPIE Proc. 825, 19 (1987).
[23] R. S. Muller and T. I. Kamins, Device Electronics for Integrated Circuits, 2nd ed. (John Wiley & Sons, New York, 1986).
[24] B. G. Streetman, Solid State Electronic Devices, 3rd ed. (Prentice Hall, Englewood Cliffs, NJ, 1990).
[25] A. Partovi, A. M. Glass, D. H. Olson, G. J. Zydzik, and K. T. Short, Opt. Lett. 17, 655 (1992).
[26] A. Partovi, A. M. Glass, G. J. Zydzik, and H. M. O'Bryan, Appl. Phys. Lett. 62, 3088 (1993).
[27] W. F. Ames, Numerical Methods for Partial Differential Equations, 2nd ed. (Academic, New York, 1977).
[28] G. D. Smith, Numerical Solution of Partial Differential Equations: Finite Difference Methods, 3rd ed. (Oxford University Press, New York, 1985).
[29] B. Landreth and G. Moddel, Appl. Opt. 31, 3937 (1992).
[30] W. P. Siegmund, in Handbook of Optics, edited by W. G. Driscoll and W. Vaughan (McGraw-Hill, New York, 1978), Sec. 13.